

CeViT: Copula-Enhanced Vision Transformer in multi-task learning and bi-group image covariates with an application to myopia screening

Chong Zhong^{1*}, Yang Li^{2*}, Jinfeng Xu^{3*}, Xiang Fu², Yunhao Liu⁴,
 Qiuyi Huang¹, Danjuan Yang⁵, Meiyan Li⁵, Aiyi Liu⁶, A.H. Welsh⁷,
 Xingtao Zhou⁵, Bo Fu², and Catherine C. Liu¹

¹Department of Data Science & Artificial Intelligence, The Hong Kong Polytechnic University

²School of Data Science, Fudan University

³Department of Biostatistics, City University of Hong Kong

⁴School of Information Science and Technology, Fudan University

⁵ Eye & ENT Hospital, Fudan University

⁶ Eunice Kennedy Shriver National Institute of Child Health and Human Development

⁷College of Business and Economics, Australian National University

Abstract

We aim to assist image-based myopia screening by resolving two longstanding problems, “how to integrate the information of ocular images of a pair of eyes”, and “how to incorporate the inherent dependence among high-myopia status and axial length for both eyes.” The classification-regression task is modeled as a novel 4-dimensional multi-response regression, where discrete responses are allowed, that relates to two dependent 3rd-order tensors (3D ultrawide-field fundus images). We present a Vision Transformer-based bi-channel architecture, named CeViT, where the common features of a pair of eyes are extracted via a shared Transformer encoder, and the interocular asymmetries are modeled through separated multilayer perceptron heads. Statistically, we model the conditional dependence among mixture of discrete-continuous responses given the image covariates by a so-called copula loss. We establish a new theoretical framework regarding fine-tuning on CeViT based on latent representations, allowing the black-box fine-tuning procedure interpretable and guaranteeing higher relative efficiency of fine-tuning weight estimation in the asymptotic setting. We apply CeViT to an annotated ultrawide-field fundus image dataset collected by Shanghai Eye & ENT Hospital, demonstrating that CeViT enhances the baseline model in both accuracy of classifying high-myopia and prediction of AL on both eyes.

Keywords: Fine-tuning, Interocular asymmetry, Large model, Relative efficiency, Representation learning.

1 Introduction

In ophthalmology research, there is a global trend to develop ocular image-based deep learning methods for ophthalmological diagnosis (Yew et al., 2024). Among ocular images, the ultra-widefield (UWF) fundus images provide a wider imaging field of view (up to 200°) on the fundus (Midena et al., 2022), and therefore motivate the development of UWF fundus-based AI methods for myopia prediction (Shi et al., 2021; Yang et al., 2022; Oh et al., 2023, among others). These methods trained convolutional neural networks (CNNs) under the empirical loss in the sense of the sum of mean squared error loss and cross entropy loss (Wang et al., 2020). However, there are still big methodological gaps between the need of ophthalmological practice and the existing methods.

- They predicted responses based on only a single-eye UWF fundus image and ad hoc tackled the “interocular asymmetry” (e.g. Engelmann et al. (2022)), neglecting the information of asymmetrical or unilateral features between a pair of eyes (Lu et al., 2022), which may lead to higher bias and false diagnostics about retinal diseases (Sankaridurg et al., 2013; Henriquez et al., 2015);
- They focused on predicting continuous labels such as spherical equivalence (SE) or/and axial length (AL), while screening of high-myopia status (1: high-myopia; 0: otherwise) is urgently needed by practicing ophthalmologists to avoid the progression of more severe diseases such as blindness (Iwase et al., 2006); and
- The use of empirical loss ignores the inherent correlation between AL and high-myopia status (Haarman et al., 2020; Zhang et al., 2024), incurring suboptimal predictive performances (Zhong et al., 2024).

This motivates us to integrate the left eye (OS) and the right eye (OD) UWF images

together and to address prediction tasks on the classification of high-myopia status of both eyes (OU) and regression of OU AL jointly. Alternatively, it calls for a multi-task learning model with *4-dimensional mixture of discrete-continuous responses* and bi-group dependent image covariates.

To the best of our knowledge, such a task is an entirely new challenge across the fields of ophthalmology, AI, and statistics. There are sporadic methods that employed OU images to predict OU labels, while they either failed to capture the common features shared by both OU ocular images into a unified neural network (Gour and Khanna, 2021; Xu and Fan, 2022), or could not predict the discrete high-myopia status (Li et al., 2024). Furthermore, for multiple mixture of discrete-continuous responses on both eyes, there are no feasible loss functions that can incorporate the conditional dependence among responses.

Besides the methodological gaps, the existing methods are all based on CNN, which is not state-of-the-art (SOTA) in computer vision tasks. Based on the breakthrough of Transformer (Vaswani et al., 2017) in natural language processing, the Vision Transformer (ViT, Dosovitskiy et al., 2020) outperforms the classical CNNs in supervise learning tasks on large-scale datasets. The ViT replaces standard convolutions by multi-head attention mechanism and hence, has a stronger capability in modeling the long-range dependencies of image patches and integrating global information (Han et al., 2022). The great success of ViT-based large models inspires its application and modification to be suitable for our ophthalmic task.

In this article, we propose Copula-enhanced Vision Transformer (CeViT), a novel multi-task learning model with bi-group image covariates. The OU UWF fundus images are separated as two groups of covariates fed to one large neural network based on the SOTA ViT, and are associated with tasks of AL regression and high-myopia classification on the

corresponding eye. The common features of OU images is aggregated by the ViT encoder as the shared feature extractor, and their heterogeneity caused by interocular asymmetries is captured by two multilayer perceptron (MLP) heads regarding both eyes. To incorporate the inter-response correlation, we develop a new loss in CeViT training based on the copula model (Sklar, 1959), which models the conditional dependence among multivariate mixture of discrete-continuous responses given the OU UWF fundus image covariates. We present a new theoretical framework to interpret the conditional dependence among responses and establish a set of inferential theories on CeViT fine-tuning in the asymptotic setting.

Our contributions in this article are tri-fold.

i) To ophthalmology, we are the first to jointly predict OU high-myopia status and AL through OU UWF fundus images; meanwhile, our proposed CeViT may be the first UWF fundus image-based AI large model for myopia screening. One challenge that hinders applying the ViT-based large model on a UWF fundus image dataset is the overfitting issue (Xiao et al., 2024), since ViT has an unprecedented model size compared with the very moderate data size of annotated UWF fundus images. We adopt the common transfer learning strategy in deep learning practice, that is, to pre-train the whole large model on a large-scale benchmark dataset, and to fine-tune a small proportion of parameters on the target small dataset (Kolesnikov et al., 2020; Djolonga et al., 2021, among others). As a result, CeViT maintains the original model size of ViT and hence gains much stronger predictive capability compared with the existing CNN-based methods.

ii) To deep learning, we make a new loss operational in Pytorch (Paszke et al., 2019), the commonly used deep learning library, based on higher-dimensional Gaussian copula density. For mixture of discrete-continuous responses, the copula-based loss in the existing literature is only applicable in bivariate cases (Zhong et al., 2024). Nonetheless, in higher-

dimensional cases (say, 4-dim for OU myopia predictions), the general formula of Gaussian copula density (Song et al., 2009) is invalid to GPU-based Pytorch as it cannot compute multivariate gaussian integral directly. We introduce a latent variable expression to the Gaussian copula density so that the log density can be expressed by a series of built-in univariate normal functions of Pytorch.

iii) To statistics, we contribute a new theoretical framework regarding fine-tuning on multi-task learning large models. Within the supervised learning context, most existing literature studied the convergence rate and excess risk bound of ReLU deep neural networks in a nonparametric regression setting (Fan et al., 2024; Shen et al., 2024; Wang et al., 2024, among others), while the multi-head attention mechanism in the ViT is NOT a ReLU neural network; within the fine-tuning context, the very limited theoretical exploration focused on pre-training data leverage (Liu et al., 2022). We formulate a general illustrative data generation model based on the concept of sufficient representations (Huang et al., 2024) in representation learning. Under the data generation model, we establish the consistency of copula estimation and asymptotic equivalence to the maximum likelihood estimator (MLE), and demonstrate the higher relative efficiency of CeViT compared with the baseline ViT trained under the empirical loss. In this sense, we might be the first to interpret the source of conditional dependence among responses in multi-task learning and study the asymptotic results of fine-tuning on ViT-based large models.

The remaining of the article is organized as follows. Section 2 presents the formulation, architecture, loss, and algorithm of CeViT. Section 3 formulates the data generation model and studies the inferential theories regarding fine-tuning on CeViT. Section 5 illustrates CeViT through simulations on synthetic data. Section 4 presents the results of applying CeViT to the UWF fundus image dataset collected by The Eye & ENT Hospital of Fudan

University. Section 6 concludes the article with brief remarks and discussions. Technical proofs and related computation details are presented in the Supplementary materials. The code for simulations is available on GitHub <https://github.com/silent618/CeViT>.

2 CeViT: architecture, loss, and algorithm

Let $\mathbf{y} = (y_1, y_2, y_3, y_4)^\top$ be the 4-dimensional vector of mixed discrete-continuous labels, where $y_1, y_3 \in \mathbb{R}$ correspond to the continuous labels of left and right eyes respectively, and $y_2, y_4 \in \{0, 1\}$ correspond to the binary labels of left and right eyes respectively. Let $\mathcal{X}_j \in \mathbb{R}^{224 \times 224 \times 3}$ be the UWF fundus images of left and right eyes respectively, for $j = 1, 2$. Let Φ be the CDF of standard normal $N(0, 1)$ and \circ be the composition of two functions. We propose the following mean regression model

$$\mathbb{E}\{\mathbf{y} | (\mathcal{X}_1, \mathcal{X}_2)\} = [g_1 \circ h(\mathcal{X}_1), \Phi \circ g_2 \circ h(\mathcal{X}_1), g_3 \circ h(\mathcal{X}_2), \Phi \circ g_4 \circ h(\mathcal{X}_2)]^\top, \quad (1)$$

where $h : \mathbb{R}^{224 \times 224 \times 2} \rightarrow \mathbb{R}^d$ denotes an encoder that projects a UWF fundus image to a d -dimensional representation vector, and $g_k : \mathbb{R}^d \rightarrow \mathbb{R}$ denotes a nonlinear function relating the representation vector to label y_k , for $k = 1, \dots, 4$. The probit link Φ can be replaced with the sigmoid link as the common fashion in classification tasks. We use the probit link for the convenience of both computation and notation.

Model (1) has two characteristics.

i) It fixes a shared encoder for both OU UWF fundus images as the representation extractor to map the images to the same representation space. This is inspired by embedding-based multi-instance learning approaches (Li et al., 2021), where the shared encoder captures the common features of both OU UWF fundus images.

ii) It forces the OU representations extracted by encoder h to contribute to the labels of

each eye separately. This is a natural setting to ensure that the labels of each eye are fully determined by the corresponding UWF fundus image. These two characteristics motivate us to consider the following bi-channel ViT architecture for CeViT.

2.1 Bi-channel ViT architecture

We present the whole architecture of CeViT in Figure 1 below. We use the state-of-the-art (SOTA) Vision Transformer (ViT) model (Dosovitskiy et al., 2020) as the backbone of CeViT. In essence, the encoder h in model (1) adopts the multiheaded self-attention mechanism (Vaswani et al., 2017) to reduce the image-specific inductive bias in feature extraction, compared with the convolutional encoder of CNNs.

The nonlinear functions g_k are separated into two MLP heads, where one outputs (g_1, g_2) , and the other outputs (g_3, g_4) . To model the correlation and heterogeneity between OU UWF fundus images simultaneously, we adopt the residual adapters (Rebuffi et al., 2017) on the MLP heads to ensure that the two MLPs share a proportion of weights. This is a fundamental difference in architecture between the proposed CeViT and OU-Copula (Li et al., 2024), where the latter imposed adapters to the convolutional blocks and share the same MLP head for both OU labels. Empirically, it seems that the structure of CeViT is more suitable to characterize the interocular asymmetries, which have been evidenced to be related to retinal diseases more than the difference between fundus images (Sankaridurg et al., 2013; Henriquez et al., 2015).

Recall that CeViT aims at predicting 4-dimensional mixture of discrete-continuous responses, we develop the following 4-dim mixed copula loss to incorporate the conditional dependence among responses given the OU UWF fundus images.

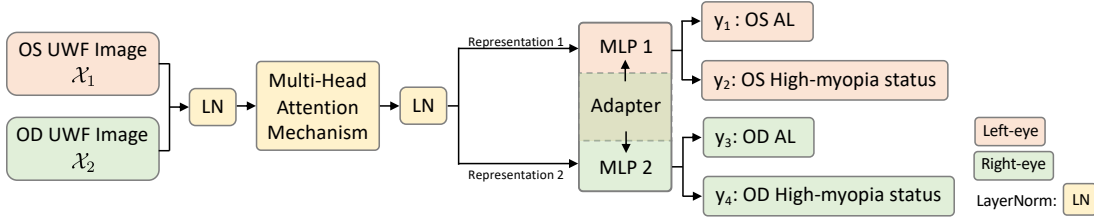


Figure 1: The bi-channel architecture of proposed CeViT.

2.2 Four-dim mixed copula loss

In the training procedure, we propose a 4-dimensional mixed copula loss to capture the dependence structure of the multivariate variable $\mathbf{y}|(\mathcal{X}_1, \mathcal{X}_2)$, as a replacement of the empirical loss widely adopted by ViT variants (Wang et al., 2020). Note that in the UWF fundus setting, it is natural to assume that the continuous responses are conditionally Gaussian (Zhong et al., 2024). Then based on model (1), we assume the conditional distribution of $\mathbf{y}|(\mathcal{X}_1, \mathcal{X}_2)$ at each margin as

$$\begin{aligned}
 y_1|\mathcal{X}_1 &\sim N(g_1 \circ h(\mathcal{X}_1), \sigma_1^2), & y_2|\mathcal{X}_1 &\sim \text{Bernoulli}(\Phi \circ g_2 \circ h(\mathcal{X}_1)), \\
 y_3|\mathcal{X}_2 &\sim N(g_3 \circ h(\mathcal{X}_2), \sigma_2^2), & y_4|\mathcal{X}_2 &\sim \text{Bernoulli}(\Phi \circ g_4 \circ h(\mathcal{X}_2)).
 \end{aligned}
 \tag{2}$$

With the conditional distribution at each margin, one can specify the joint distribution of $\mathbf{y}|(\mathcal{X}_1, \mathcal{X}_2)$ through a Gaussian copula.

We first present the latent variable expressions for the discrete variables y_2 and y_4 . Without ambiguity, let $\mu_1 := g_1 \circ h(\mathcal{X}_1), \mu_2 := g_3 \circ h(\mathcal{X}_2), \mu_3 := g_2 \circ h(\mathcal{X}_1), \mu_4 := g_4 \circ h(\mathcal{X}_2)$. Let $u_3, u_4 \sim N(0, 1)$ be two latent variables that are marginally standard normal. Let $X \stackrel{d}{=} Y$ be the equality in distribution between random variables X and Y . We immediately have the following marginal distributions

$$y_2|\mathcal{X}_1 \stackrel{d}{=} I(u_3 \geq -\mu_3), \quad y_4|\mathcal{X}_2 \stackrel{d}{=} I(u_4 \geq -\mu_4).
 \tag{3}$$

Let $\mathbf{u} = [(y_1|\mathcal{X}_1), (y_3|\mathcal{X}_2), u_3, u_4]^\top := (u_1, u_2, u_3, u_4)^\top$. The joint distribution of $\mathbf{y}|(\mathcal{X}_1, \mathcal{X}_2)$ is fully determined by the joint distribution of \mathbf{u} , which is distributed as multivariate normal

$\text{MVN}_4\{(\mu_1, \mu_2, 0, 0)^\top, \Sigma = \text{diag}(\sigma_1, \sigma_2, 1, 1) \Gamma \text{diag}(\sigma_1, \sigma_2, 1, 1)\}$, where

$$\Gamma = \begin{pmatrix} 1 & \rho_{12} & \rho_{13} & \rho_{14} \\ \rho_{12} & 1 & \rho_{23} & \rho_{24} \\ \rho_{13} & \rho_{23} & 1 & \rho_{34} \\ \rho_{14} & \rho_{24} & \rho_{34} & 1 \end{pmatrix} := \begin{pmatrix} \Gamma_{11} & \Gamma_{12} \\ \Gamma_{21} & \Gamma_{22} \end{pmatrix}, \Gamma_{ij} \in \mathbb{R}^{2 \times 2}, i, j = 1, 2.$$

We call $\mathcal{C} = \{\sigma_1, \sigma_2, \rho_{sj}, s, j = 1, \dots, 4, s \neq j\}$ the set of copula parameters. Let $\Phi_2[(\cdot, \cdot); \boldsymbol{\mu}, V]$ be the joint CDF of $\text{MVN}_2(\boldsymbol{\mu}, V)$. Based on the above notation, the log density of $\mathbf{y}|(\mathcal{X}_1, \mathcal{X}_2)$ is given by the following theorem.

Theorem 1. *Under mean regression (1) and marginal model (2), the joint log density of $\mathbf{y}|(\mathcal{X}_1, \mathcal{X}_2)$ is*

$$\begin{aligned} l\{\mathbf{y}|(\mathcal{X}_1, \mathcal{X}_2)\} = & -\frac{1}{2(1-\rho^2)} \left\{ \frac{(y_1 - \mu_1)^2}{\sigma_1^2} - \frac{2\rho(y_1 - \mu_1)(y_3 - \mu_2)}{\sigma_1\sigma_2} + \frac{(y_3 - \mu_2)^2}{\sigma_2^2} \right\} \\ & + \log [y_4(1 - 2y_2)\Phi(-\mu_3; \tilde{\mu}_1; \tilde{v}_{11}) + y_4(1 - 2y_2)\Phi\{-\mu_4; \tilde{\mu}_2; \tilde{v}_{22}\} \\ & + (1 - 2y_2)(1 - 2y_4)\Phi_2\{(-\mu_3, -\mu_4)^\top; \tilde{\boldsymbol{\mu}}, \tilde{V}\} + y_2y_4] + C, \end{aligned} \quad (4)$$

where $\tilde{\boldsymbol{\mu}} = (\Gamma_{21}\Gamma_{11}^{-1}(\sigma_1^{-1}(y_1 - \mu_1), \sigma_2^{-1}(y_3 - \mu_2)))^\top := (\tilde{\mu}_1, \tilde{\mu}_2)^\top$, $\tilde{V} = \Gamma_{22} - \Gamma_{21}\Gamma_{11}^{-1}\Gamma_{12}$, and C is the normalization constant.

Let n be the data size. Let $\mathcal{D} = \{\mathbf{y}_i, \mathcal{X}_{i1}, \mathcal{X}_{i2}\}_{i=1}^n$ be the dataset of training labels and training images. Let \mathbf{W} be the weights of CeViT. Based on Theorem 1, the copula loss function is given by the minus log likelihood

$$\mathcal{L}\{\mathbf{W}|(\mathcal{D}, \mathcal{C})\} = \sum_{i=1}^n -l\{\mathbf{y}_i|(\mathcal{X}_{i1}, \mathcal{X}_{i2})\}. \quad (5)$$

Since PyTorch does not compute CDF Φ_2 directly, we realize copula loss (5) by transforming Φ_2 into products of Φ in PyTorch to guarantee the gradient is stored on GPU; refer to Supplement B.1 for details.

2.3 Feasible CeViT algorithm

The proposed copula loss (5) relies on the known copula parameters \mathcal{C} . In practice, since \mathcal{C} is unknown, one has to either estimate \mathcal{C} first, or employ alternating methods to update \mathbf{W} and \mathcal{C} iteratively. Due to the extremely large model size of ViT, alternating methods incur a heavy computation burden and unstable fine-tuning. Hence, we tend to estimate \mathcal{C} first and then use the estimator $\hat{\mathcal{C}}$ replace the unknown copula parameters. Such a spirit is similar to the feasible generalized least squares (FGLS) estimator (Avery, 1977). Therefore, we call our algorithm Feasible CeViT algorithm.

Let $\mathcal{L}_0(\mathbf{W}|\mathcal{D})$ be the empirical loss

$$\sum_{i=1}^n \{y_{i1} - g_1 \circ h(\mathcal{X}_{i1})\}^2 + \{y_{i3} - g_3 \circ h(\mathcal{X}_{i2})\}^2 + \text{BCE}(g_2; y_{i2}, \mathcal{X}_{i1}) + \text{BCE}(g_4; y_{i4}, \mathcal{X}_{i2}), \quad (6)$$

where $\text{BCE}(g; y, \mathcal{X}) = y \log\{\Phi \circ g \circ h(\mathcal{X})\} + (1 - y) \log\{1 - \Phi \circ g \circ h(\mathcal{X})\}$ denotes the binary cross entropy loss. A warm-up CeViT model is obtained by optimizing the empirical loss (6), with the fitted encoder and nonlinear functions denoted by \hat{h}_0 and \hat{g}_{0k} for $k = 1, \dots, 4$, respectively. Then the empirical estimator $\hat{\mathcal{C}}$ for copula parameters \mathcal{C} is straightforward.

Let $\text{corr}(\cdot, \cdot)$ be the correlation operator between two variables. The latent variable expression (3) indicates that $\rho_{sj} = \text{corr}(u_s, u_j)$, for $s, j = 1, \dots, 4$. Let $R(\cdot, \cdot)$ be the sample correlation operator between two samples and SD be the sample standard deviation. The empirical estimator $\hat{\mathcal{C}}^{emp}$ is given as

$$\begin{aligned} \hat{\sigma}_1 &= \text{SD}\{y_{i1} - \hat{g}_{01} \circ \hat{h}_0(\mathcal{X}_{i1})\} := \text{SD}(e_{i1}), \hat{\sigma}_2 = \text{SD}\{y_{i3} - \hat{g}_{03} \circ \hat{h}_0(\mathcal{X}_{i2})\} := \text{SD}(e_{i2}), \\ \hat{\rho}_{12} &= R(\mathbf{e}_1, \mathbf{e}_2), \quad \hat{\rho}_{34} = R\{\hat{g}_{02} \circ \hat{h}_0(\mathcal{X}_{i1}), \hat{g}_{04} \circ \hat{h}_0(\mathcal{X}_{i2})\}, \\ \hat{\rho}_{t,j+2} &= R\{e_{it}, -\Phi^{-1}(\mathcal{S} \circ \hat{\mu}_{i,j+2})\}, \quad t, j, = 1, 2. \end{aligned} \quad (7)$$

The final round training of CeViT is conducted by optimizing the copula loss $\mathcal{L}\{\mathbf{W}|(\mathcal{D}, \hat{\mathcal{C}}^{emp})\}$.

We summarize the whole feasible CeViT algorithm in Algorithm 1.

Algorithm 1 Feasible CeViT algorithm

Input: Training data \mathcal{D} ; data size n .

Output: Fitting CeViT with weights $\hat{\mathbf{W}}$ trained under the 4-dimensionl copula loss.

- 1: Fit the warm-up ViT model by optimizing empirical loss (6): $\hat{\mathbf{W}}_0 = \arg \min_{\mathbf{W}} \mathcal{L}_0(\mathbf{W}|\mathcal{D})$ on GPU.
 - 2: Obtain empirical estimator of copula parameters $\hat{\mathcal{C}}^{emp}$ by (7) on CPU.
 - 3: Fit the CeViT model by optimizing copula loss (5): $\hat{\mathbf{W}} = \arg \min_{\mathbf{W}} \mathcal{L}\{\mathbf{W}|(\mathcal{D}, \hat{\mathcal{C}}^{emp})\}$ on GPU.
-

3 Theory

In this section, we establish the theoretical framework of fine-tuning on CeViT in the asymptotic setting. We formulate an illustrative data generation model with latent representations for CeViT in Section 3.1, and establish the inferential theories regarding fine-tuning in Section 3.2.

3.1 Illustrative data generation model

We start from rewriting CeViT into Linear ViT, an illustrative model with a linear structure, while maintaining the model complexity of ViT to match the fine-tuning fashion.

Linear ViT: fine-tuning and identifiability

Based on mean regression (1), Linear ViT is formulated as

$$\mathbb{E}\{\mathbf{y}|(\mathcal{X}_1, \mathcal{X}_2)\} = [\boldsymbol{\beta}_1^\top \tilde{h}(\mathcal{X}_1), \Phi\{\boldsymbol{\beta}_2^\top \tilde{h}(\mathcal{X}_1)\}, \boldsymbol{\beta}_3^\top \tilde{h}(\mathcal{X}_2), \Phi\{\boldsymbol{\beta}_4^\top \tilde{h}(\mathcal{X}_2)\}]^\top, \quad (8)$$

where $\tilde{h} : \mathbb{R}^{224 \times 224 \times 3} \rightarrow \mathbb{R}^{d_0}$ is a transformed encoder, acting the same role of encoder h in model (1), and $\boldsymbol{\beta}_k \in \mathbb{R}^{d_0}$ are the coefficient vectors corresponding to the representation vectors extracted by encoder \tilde{h} . The formulation of Linear ViT (8) is motivated by the architecture of ViT, where the MLP heads contain only two hidden layers (Dosovitskiy et al., 2020). Let $\text{GELU}(x) = x\Phi(x)$ be the Gaussian Error Linear Unit (GELU) function

(Hendrycks and Gimpel, 2016). With the ViT backbone, Linear ViT (8) is equivalent to model (1) if $\tilde{h}(\mathcal{X}) = \text{GELU}\{\boldsymbol{\gamma}^\top h(\mathcal{X})\}$, where $\boldsymbol{\gamma} \in \mathbb{R}^{d \times d_0}$ denotes the weight matrix of the first hidden layer of MLP heads of ViT.

In model (8), the coefficients $\boldsymbol{\beta}_k$ are identifiable if and only if the encoder \tilde{h} is fixed. This condition is (almost) satisfied if one fine-tunes the ViT by Low-Rank Adaptation (LoRA, Hu et al., 2022), the commonly used fine-tuning tool for large models. Let $\mathbf{W}_{\tilde{h}} \in \mathbb{R}^{p_1 \times p_2}$ be the weight matrix of \tilde{h} , where $p_1, p_2 \gg n$ are two extremely large number. Let $\mathbf{W}_{\tilde{h}_0}$ be the weights of pre-trained encoder \tilde{h}_0 . With LoRA, the weight matrix $\mathbf{W}_{\tilde{h}}$ is updated by

$$\mathbf{W}_{\tilde{h}} = \mathbf{W}_{\tilde{h}_0} + BA,$$

where $B \in \mathbb{R}^{p_1 \times r}$, $A \in \mathbb{R}^{r \times p_2}$ are rank- r matrices with r being a small number (e.g. $r = 8$ in our numerical studies). Based on the guidance in Dosovitskiy et al. (2020, Section 3.1), when using LoRA to fine-tune the ViT, one freezes $\mathbf{W}_{\tilde{h}_0}$, and conducts full-parameter fine-tuning on the last hidden layer i.e. $\boldsymbol{\beta}_k$ for $k = 1, \dots, 4$, and low-rank matrices A and B . Consequently, we conclude that in the fine-tuning procedure, the transformed encoder $\tilde{h} \approx \tilde{h}_0$, that is, \tilde{h} is almost fixed.

Latent sufficient representation

Under model (8), we introduce the concept of latent sufficient representation based on the following assumptions.

Assumption 1 (Sufficient representation). *Under model (8), the encoder \tilde{h} is a sufficient representation of \mathcal{X}_1 and \mathcal{X}_2 such that*

$$\mathbf{y} \perp (\mathcal{X}_1, \mathcal{X}_2) | \{\tilde{h}(\mathcal{X}_1), \tilde{h}(\mathcal{X}_2)\}.$$

Assumption 2 (Finite second moment). *Under Assumption 1, $\mathbb{E}\|\tilde{h}(\mathcal{X}_j)\|^2 < \infty$, for $j = 1, 2$.*

Assumption 1 is a bivariate version of the definition of sufficient representation (Huang et al., 2024) in the sense that it requires sufficient representations on both image covariates \mathcal{X}_1 and \mathcal{X}_2 . Such formulation can be viewed as a nonparametric extension of the sufficient dimension reduction (Li, 2018, Sec 2.2). Since the attention-based transformer encoder is the SOTA in both supervised and generative learning tasks, it is reasonable to assume the ViT encoder is a sufficient representation of UWF fundus images \mathcal{X}_1 and \mathcal{X}_2 . Assumption 2 is a general assumption for sufficient representation (Huang et al., 2024, Lemma 1).

Lemma 1 (Latent sufficient representation). *Assume model (8). Assume Assumptions 1 and 2. Given encoder \tilde{h} and images \mathcal{X}_1 and \mathcal{X}_2 , there exist latent variables $\mathbf{Z}_1, \mathbf{Z}_2, \mathbf{Z}_3, \mathbf{Z}_4 \in \mathbb{R}^{d_0}$ such that*

$$\mathbf{y} \perp (\mathcal{X}_1, \mathcal{X}_2) | (\mathbf{Z}_1, \mathbf{Z}_2, \mathbf{Z}_3, \mathbf{Z}_4),$$

and their conditional distribution is

$$(\mathbf{Z}_1^\top, \dots, \mathbf{Z}_4^\top)^\top | (\mathcal{X}_1, \mathcal{X}_2) \sim \text{MVN} \left[\{\tilde{h}(\mathcal{X}_1)^\top, \tilde{h}(\mathcal{X}_1)^\top, \tilde{h}(\mathcal{X}_2)^\top, \tilde{h}(\mathcal{X}_2)^\top\}^\top, \Sigma_{\mathbf{Z}} := \Sigma_{ij}^{4 \times 4} \right],$$

with $\Sigma_{ij} \in \mathbb{R}^{d_0 \times d_0}$ for $i, j = 1, \dots, 4$, such that $\Sigma_{\mathbf{Z}} \in \mathbb{R}^{(4d_0) \times (4d_0)}$ is positive definite.

We call the latent variables $\mathbf{Z} := (\mathbf{Z}_1, \dots, \mathbf{Z}_4)$ latent sufficient representation of \mathcal{X}_1 and \mathcal{X}_2 . Lemma 1 presents the form of the posterior distribution of latent sufficient representation \mathbf{Z} . It is inspired by Huang et al. (2024, Lemma 1), which states that in priori $\mathbf{Z}_j \sim \text{MVN}(\mathbf{0}_{d_0}, \mathbf{I}_{d_0})$ marginally for $j = 1, \dots, 4$. In practice, the latent sufficient representation may be interpreted as a variational autoencoder, whose posterior conditional on the images covariates is commonly approximated by a multivariate normal distribution (Cinelli et al., 2021, Sec 5.5).

Data generation model: generalized linear model with latent covariates

Denote the marginal variance of $y_1|\mathcal{X}_1$ and $y_3|\mathcal{X}_2$ as σ_1 and σ_2 respectively. Under Lemma 1, let $\sigma_1^2 = \|\beta_1\|_2^{-2}\sigma_{1A}^2 + \sigma_{1B}^2$, $\sigma_2^2 = \|\beta_3\|_2^{-2}\sigma_{2A}^2 + \sigma_{2B}^2$; let $\Sigma_{11} = \sigma_{1A}^2\mathbf{I}_{d_0}$, $\Sigma_{22} = \|\beta_2\|_2^{-2}\mathbf{I}_{d_0}$, $\Sigma_{33} = \sigma_{2A}^2\mathbf{I}_{d_0}$, $\Sigma_{44} = \|\beta_4\|_2^{-2}\mathbf{I}_{d_0}$. Let $\tilde{y}_2 := \beta_2^\top \mathbf{Z}_2$, $\tilde{y}_4 := \beta_4^\top \mathbf{Z}_4$. One can rewrite model (8) as an equivalent data generation model of \mathbf{y} through latent sufficient representation \mathbf{Z} . At each margin, the data generation model is

$$\begin{aligned} y_1|\mathbf{Z} &= \beta_1^\top \mathbf{Z}_1 + \epsilon_1, & y_2|\mathbf{Z} &= I(\tilde{y}_2 \leq 0), \\ y_3|\mathbf{Z} &= \beta_3^\top \mathbf{Z}_3 + \epsilon_3, & y_4|\mathbf{Z} &= I(\tilde{y}_4 \leq 0), \end{aligned} \tag{9}$$

where $(\epsilon_1, \epsilon_3) \sim \text{MVN}(\mathbf{0}_2, \Sigma_\epsilon)$ with $\text{diag}(\Sigma_\epsilon) = (\sigma_{1B}^2, \sigma_{2B}^2)^\top$.

Data generation model (9) indicates the following conditional covariance structure among responses given the images $\mathcal{X} := (\mathcal{X}_1, \mathcal{X}_2)$. Without loss of generality, assume Σ_ϵ is an orthogonal matrix. Take the pair-wise conditional covariance between y_1 and other responses for example, we have

$$\text{Cov}\{(y_1, y_3)|\mathcal{X}\} = \beta_1^\top \Sigma_{13} \beta_3, \text{Cov}\{(y_1, \tilde{y}_2)|\mathcal{X}\} = \beta_1^\top \Sigma_{12} \beta_2, \text{Cov}\{(y_1, \tilde{y}_4)|\mathcal{X}\} = \beta_1^\top \Sigma_{14} \beta_4. \tag{10}$$

Covariance structure (10) illustrates the generalization of data generation model (9). By setting the sub-matrices in $\Sigma_{\mathbf{Z}}$ to be zeros, model (9) reduces to the cases where labels are conditionally independent given images \mathcal{X} , and hence the copula loss reduces to the empirical loss. Furthermore, data generation model (9) interprets the conditional dependence among responses from the covariance structure of the latent sufficient representations. To the best of our knowledge, we might be the first to clarify the source of such conditional dependence in deep learning, though the existence has been empirically demonstrated by Zhong et al. (2024) and Li et al. (2024). This enables us to establish a thorough theoretical

framework in fine-tuning to understand the enhancement by incorporating the conditional dependence.

3.2 Statistical inference of fine-tuning on CeViT

In feasible CeViT algorithm 1, the final output of CeViT relies on the empirical estimator $\hat{\mathcal{C}}$ in (7) for the copula parameters. A basic concern is the consistency of $\hat{\mathcal{C}}$. The following theorem states that all elements in $\hat{\mathcal{C}}$ are \sqrt{n} -consistent.

Theorem 2 (Copula consistency). *Assume data generation model (9). Under empirical loss \mathcal{L}_0 given by (6), as data size $n \rightarrow \infty$, we have $|\hat{\sigma}_j^{emp} - \sigma_j| = O_p(n^{-1/2})$, for $j = 1, 2$, and $|\hat{\rho}_{st}^{emp} - \rho_{st}| = O_p(n^{-1/2})$, for $s, j = 1, \dots, 4, s \neq t$.*

Theorem 2 is a consequence of the consistency of the M-estimator. Such consistency enables us to establish the asymptotic equivalence to the MLE, since the copula loss is a minus of log likelihood. Although the latent marginal expression in model (3) is slightly different from data generation model (9), their likelihood functions are mathematically equivalent by some notation translation. Hence, without ambiguity, we denote the log likelihood under data generation model (9) by $l\{\boldsymbol{\beta}|\mathcal{D}, \mathcal{C}\}$, and denote the corresponding copula loss by \mathcal{L} hereafter.

Let $\hat{\boldsymbol{\beta}}^{fes} := \arg \min_{\boldsymbol{\beta}} \mathcal{L}\{\boldsymbol{\beta}|\mathcal{D}, \hat{\mathcal{C}}^{emp}\}$ be the feasible estimator of $\boldsymbol{\beta}$ obtained by feasible CeViT algorithm 1. The following theorem states the asymptotic equivalence of the feasible estimator to the MLE. The dimension d_0 of $\boldsymbol{\beta}$ is assumed to be a fixed number, as the default setting of ViT.

Theorem 3 (Asymptotic MLE equivalence). *Assume data generation model (9). As data size $n \rightarrow \infty$, the feasible estimator $\hat{\boldsymbol{\beta}}^{fes}$ is asymptotic equivalent to the MLE $\hat{\boldsymbol{\beta}}^{mle} := \arg \min_{\boldsymbol{\beta}} \mathcal{L}(\boldsymbol{\beta}|\mathcal{D}, \mathcal{C})$, in the sense that $\|\hat{\boldsymbol{\beta}}^{fes} - \hat{\boldsymbol{\beta}}^{mle}\|_2 = O_p(n^{-1/2})$.*

Theorem 3 is a ViT fine-tuning version of the asymptotic equivalence of feasible generalized least square estimator (Prucha, 1984) and hence, justifies the feasible CeViT algorithm.

The remaining and natural question is “does the copula loss outperform the empirical loss in CeViT fine-tuning?” Or equivalently, “does incorporating the conditional dependence information help fine-tuning?” The following theorem compares the relative efficiency between the estimators obtained under these two loss functions. Since the empirical loss is closely related to the least square loss, we denote the estimator obtained under the empirical loss by $\hat{\beta}^{ols}$.

Theorem 4 (Relative efficiency). *Assume data generation model (9). As data size $n \rightarrow \infty$, we have $Eff(\hat{\beta}^{fes}) \geq Eff(\hat{\beta}^{ols})$.*

Theorem 4 justifies the utility of the proposed copula loss in ViT fine-tuning from the perspective of higher relative efficiency. Theorem 4 has two improvements compared to Zhong et al. (2024, Theorem 1): 1) Theorem 4 is applied to cases of 4-dimensional mixture of discrete-continuous responses, while the latter is limited to the cases of bi-variate purely continuous responses; 2) Theorem 4 does not rely on those tricky assumptions on the feature maps, which cannot be validated and may even be unrealistic. The difference is due to the different interpretations to the conditional dependence among responses given the image covariates. For purely continuous responses, Zhong et al. (2024) assumes the conditional dependence structure of $\mathbf{y}|\mathcal{X}$ comes from the independent model noises; for mixture of discrete-continuous responses, Zhong et al. (2024) fails to interpret the source of such conditional dependence. In contrast, with latent sufficient representations, model (9) allows that both the mean function and the conditional dependence structure contain the information of β . Therefore, by incorporating the conditional dependence, the copula loss leads to higher relative efficiency of β^{fes} .

4 Application on the UWF fundus image dataset

In this section, we apply CeViT to our annotated UWF fundus image dataset for myopia screening tasks.

Dataset The Eye and ENT Hospital of Fudan University has collected 5228 UWF fundus images from the eyes of 2614 patients using the Optomap Daytona scanning laser ophthalmoscope (Daytona, Optos, UK), from December 2014 to June 2020. All enrolled patients sought refractive surgery treatment and were exclusively myopia patients. Each patient has four labels tested as the ground truth: the AL of OU and the OU high myopia status (1: high myopia; 0, otherwise). The UWF fundus images obtained during the study are exported in 3-channel JPEG format and compressed to a resolution of 224 x 224 pixels to facilitate subsequent analysis.

Methods for comparison We compare the performances of several large models: i) ViT, the basic ViT backbone which is trained under the empirical loss (6); ii) CeViT, the basic ViT backbone which is trained under the copula loss (5); iii) CeViT-A, adapters added to the MLP heads of the basic ViT backbone, which is trained under the copula loss (5).

Experiment setup and evaluation metrics We conduct 4 runs of 5-fold cross-validation on the UWF dataset. For continuous responses (OU AL), we use mean square error (MSE) as the evaluation metric; for discrete responses (OU high-myopia status), we use the classification accuracy and the areas under curve (AUC) as the evaluation metrics.

Implementation details We select the ViT baseline model pre-trained on ImageNet-21k as the pre-trained model, and apply LoRA in fine-tuning with the rank set as $r = 8$. For CeViT and CeViT-A, both Steps 1 and 3 in Algorithm 1 consist of 50 epochs to guarantee convergence. A batch size of 129 was used throughout the training on all models. We utilize the Adam optimizer and employed PyTorch’s StepLR as the learning rate scheduler.

For ViT training (and warm-up ViT training in both CeViT and CeViT-A), the initial learning rate is set to 10^{-3} , which decay by a factor of 0.9 every 4 epochs. In Step 3 of Algorithm 1 for the training of CeViT and CeViT-A, the initial learning rate is adjusted to 10^{-4} , decaying by a factor of 0.9 every two epochs.

Considering the heterogeneity caused by interocular asymmetry in medical images, which is relatively small but not negligible, we set a smaller value $\hat{d}=1$ for the intermediate dimension \hat{d} of the adapter bottleneck. Regarding the choice of insertion layers and the scaling factor for the adapter modules, we follow the recommendations from AdaptFormer (Chen et al., 2022), inserting adapters into each Transformer block and setting the scaling factor to 0.1 to ensure the model could effectively capture features and adapt to new task requirements.

We conduct parallel training using three RTX 4090 GPUs, and the entire training process takes approximately 4.5 hours to complete.

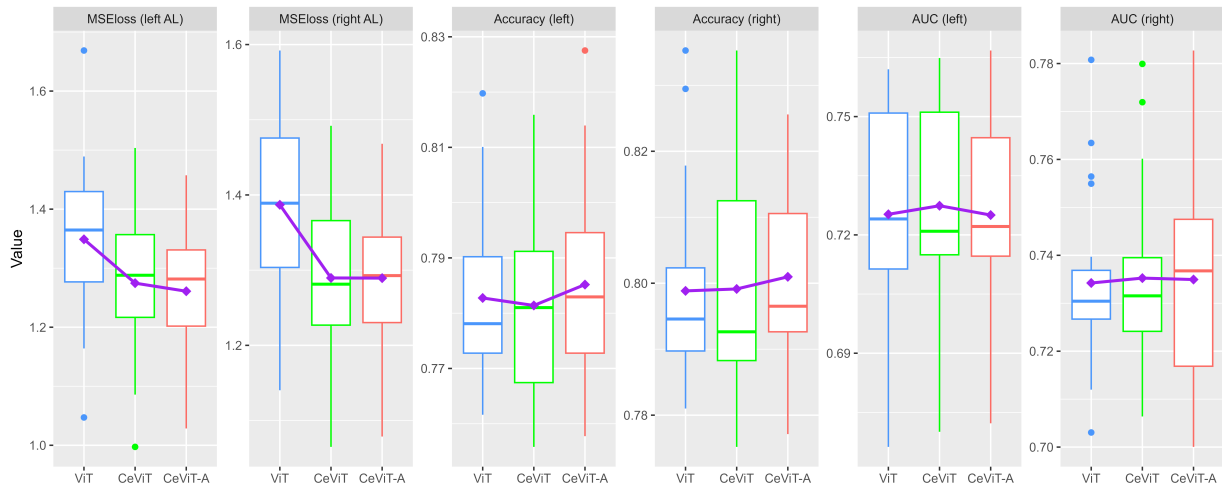


Figure 2: Boxplots of evaluation metrics among 4 runs of 5-fold CV on the UWF fundus image dataset. The average metrics are labeled as polylines.

Results Figure 2 presents the boxplots of evaluation metrics. For regression tasks, the

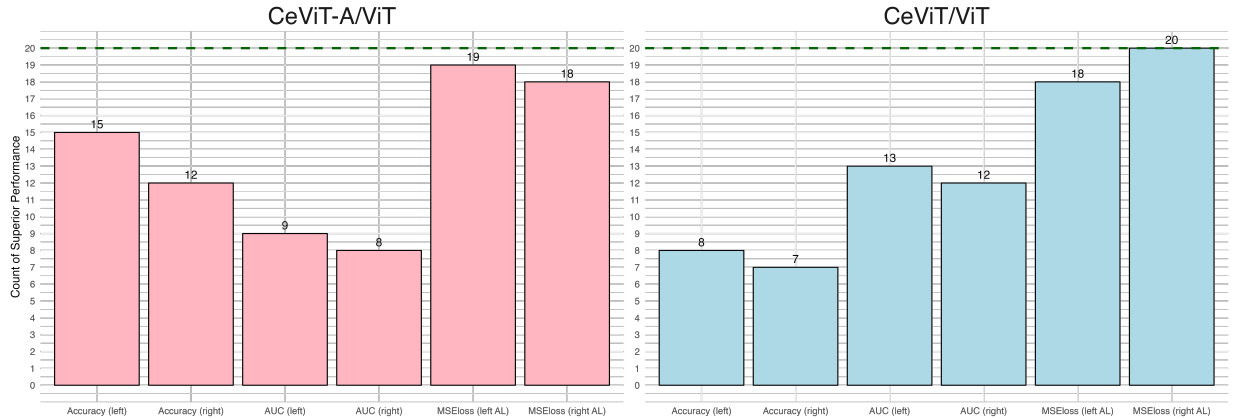


Figure 3: Win count of CeViT and CeViT-A compared with the baseline ViT on different evaluation metrics.

boxplots show that both CeViT and CeViT-A absolutely reduce the prediction MSE of OU AL compared with the baseline ViT. The significance of improvements in OU AL prediction can be evidenced by Figure 3, which presents the win count plot of CeViT and CeViT-A against the baseline ViT in all 20 folds of testing. This result demonstrates the effectiveness of copula loss in enhancing the baseline ViT on regression tasks. For classification tasks, all three methods are comparable in both accuracy and AUC, where CeViT-A slightly outperforms. This result supports the use of adapters. We conjecture there are two reasons for the mere enhancement of classification tasks of CeViT and CeViT-A. 1) The ViT pre-trained on ImageNet-21k may not be the best choice to train UWF fundus images for classification, and hence on our UWF dataset, the ViT backbone has reached its predictive upper-bound, which cannot be enhanced through fine-tuning; 2) The copula loss (5) is much more complex than the empirical loss (6), especially on the classification tasks; therefore, optimizing the copula loss may increase the optimization error, though it reduces the statistical error; according to the well-known excess risk decomposition (Teng et al., 2022), such a trade-off may hinder the copula loss enhancing the classification accuracy.

5 Simulation

In this section, we carry out simulations to further illustrate CeViT and the proposed copula loss through synthetic data. We generate 15000 pairs of synthetic images (X_1, X_2) to simulate the OU UWF fundus images, and generate the corresponding discrete-continuous responses to simulate the OU High-myopia status and OU AL. We conduct 5-fold CV for evaluation.

The synthetic images are generated as $X_1, X_2 \in \mathbb{R}^{72 \times 72}$ such that for $j = 1, 2$,

$$X_j = \begin{pmatrix} X_{j,1,1} & X_{j,1,2} & X_{j,1,3} \\ X_{j,2,1} & X_{j,2,2} & X_{j,2,3} \\ X_{j,3,1} & X_{j,3,2} & X_{j,3,3} \end{pmatrix}, \quad X_{j,t,s} \in \mathbb{R}^{24 \times 24} := X_{j,t,s}^{(k,l)}, \quad t, s = 1, 2, 3, \quad k, l = 1, \dots, 24.$$

For $k, l = 1, \dots, 24$, we set

$$\begin{pmatrix} X_{1,3,3}^{(k,l)} \\ X_{2,3,3}^{(k,l)} \end{pmatrix} \sim \text{MVN} \left\{ \begin{pmatrix} 0.5 \\ 0.5 \end{pmatrix}, \begin{pmatrix} \frac{1}{4} & \frac{1}{8} \\ \frac{1}{8} & \frac{1}{4} \end{pmatrix} \right\}$$

as elements of the bright block and

$$\begin{pmatrix} X_{1,t,s}^{(k,l)} \\ X_{2,t,s}^{(k,l)} \end{pmatrix} \sim \text{MVN} \left\{ \begin{pmatrix} 0 \\ 0 \end{pmatrix}, \begin{pmatrix} \frac{1}{4} & \frac{1}{8} \\ \frac{1}{8} & \frac{1}{4} \end{pmatrix} \right\}$$

as elements of the dark blocks, for $(t, s) \neq (3, 3)$. Under this setting, the two images are themselves correlated. Let responses $y_1, y_3 \in \mathbb{R}$ represent the regression tasks, and $y_2, y_4 \in \{0, 1\}$ represent the classification tasks. Similar to the real data setting, the pair (y_1, y_2) corresponds to X_1 only, and the pair (y_3, y_4) corresponds to X_2 only. We generate the responses as follows.

$$y_1 = \sum_{1 \leq t, s \leq 3} S_{t,s}(X_{1,t,s}) + e_1, \quad y_3 = \sum_{1 \leq t, s \leq 3} S_{t,s}(X_{2,t,s}) + e_3,$$

$$y_2 \sim \text{Bernoulli} \left[\mathcal{S} \left\{ \sum_{1 \leq t, s \leq 3} S_{t,s}^*(X_{1,t,s}) \right\} + e_2 \right], \quad y_4 \sim \text{Bernoulli} \left[\mathcal{S} \left\{ \sum_{1 \leq t, s \leq 3} S_{t,s}^*(X_{2,t,s}) \right\} + e_4 \right],$$

where $\mathbf{e} := (e_1, e_2, e_3, e_4)^\top \sim \text{MVN}(\mathbf{0}_4, \Sigma_e)$, \mathcal{S} denotes the Sigmoid function, and $S_{t,s}$ and $S_{t,s}^*$ are block operators on block (t, s) . We set the covariance matrix as

$$\Sigma_e = \begin{pmatrix} 1 & 1/2 & 1/2 & 1/8 \\ 1/2 & 1 & 1/8 & 1/2 \\ 1/2 & 1/8 & 1 & 1/2 \\ 1/8 & 1/2 & 1/2 & 1 \end{pmatrix}.$$

We define the block operators as follows

$$S_{1,1} = \sum_{1 \leq k, l \leq 3} \tanh(X_{j,1,1}^{(k,l)}), \quad S_{2,2} = \sum_{1 \leq k, l \leq 3} X_{j,2,2}^{(k,l)}, \quad S_{3,3} = \tanh \left\{ \sum_{1 \leq k, l \leq 3} X_{j,3,3}^{(k,l)} \right\}, \quad j = 1, 2,$$

and $S_{t,s} = 0$ for other blocks. For the block operators $S_{t,s}^*$, we set

$$S_{2,2}^* = S_{2,2} = \sum_{1 \leq k, l \leq 3} X_{j,2,2}^{(k,l)}, \quad j = 1, 2,$$

and $S_{t,s}^* = 0$ for other blocks. This setting guarantees that marginally $E(y_2) = E(y_4) = 1/2$, a set of balance labels.

In our simulations, we compare CeViT with the baseline ViT, with the evaluation metrics following that were used in Section 4. From Figure 4, we find that CeViT significantly outperforms in regression tasks for (simulated) OU AL predictions, and significantly enhances the accuracy in the classification of (simulated) left eye high-myopia status; CeViT also moderately enhances the baseline on other metrics. These results demonstrate the generalization ability of CeViT on the synthetic dataset.

6 Discussion

In this article, we address high-myopia screening and AL predictions of both eyes based on OU UWF fundus images. We propose CeViT, a novel bi-channel ViT-based large model

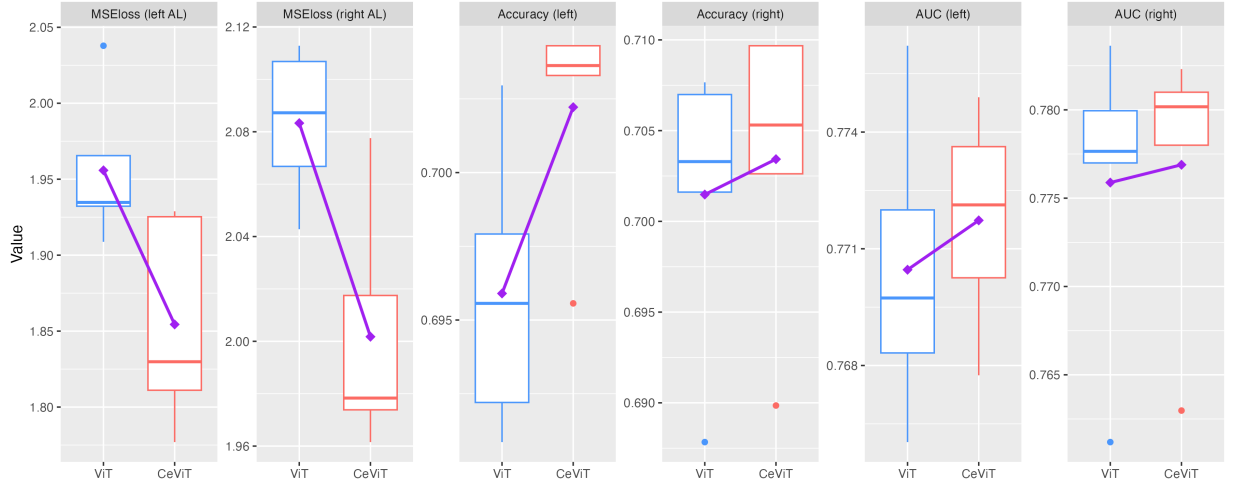


Figure 4: Boxplots of evaluation metrics on synthetic datasets. The average metrics are labeled as polylines.

that captures the correlation and heterogeneity of UWF images of a pair of eyes simultaneously. With 4-dimensional mixture of discrete-continuous responses, we theoretically and empirically demonstrate the proposed copula loss outperforms the empirical loss in ViT fine-tuning. As a result, on our UWF fundus image dataset, CeViT (baseline ViT trained under the copula loss) with adapters on MLP sharply strengthens the baseline ViT in AL prediction, and moderately enhances the classification accuracy in high-myopia status.

The proposed CeViT is an upgraded version of both CeCNN (Zhong et al., 2024) and OU-Copula (Li et al., 2024).

i) Compared with CeCNN, CeViT integrates the information of OU UWF images (induced 4-dim multi-responses) rather than a single-eye image (bi-variate responses). In a more complicated scenario, this article presents a new theoretical framework based on latent representations in illustrative data generation model (9), where the conditional dependence among responses is naturally attributed to the covariance structure of latent representations; while CeCNN cannot interpret the source of conditional dependence. In

this sense, this article *make the black-box ViT model fine-tuning interpretable*. In addition, by Theorem 1, the proposed copula loss is more general, since it reduces to that of CeCNN by specifying $\rho_{12} = \rho_{23} = \rho_{14} = 0$.

ii) Compared with OU-Copula, CeViT is more capable to handle both classification and regression tasks. The proposed copula loss reduces to the logarithm of multivariate normal density used by OU-Copula if the responses are all continuous. The asymptotic higher relative efficiency under the copula loss also holds on purely continuous cases; refer to the proof of Theorem 4 in Supplement A.4 for details.

iii) CeViT employs the SOTA ViT backbone and hence enjoys a higher predictive capability than both OU-Copula and CeCNN, which are based on classical CNN e.g. the ResNet (He et al., 2016). Table 1 shows that ViT-based models have lower MSE of both OU AL, and higher accuracy on left eye high-myopia classification on the same UWF dataset compared with the existing CNN-based methods. These results justify the use of the ViT backbone for its superiority in both regression and classification tasks.

Table 1: Comparison between average evaluation metrics (standard deviation in bracket) of CeViT and CNN-based methods on the same UWF dataset.

Methods	Regression		Methods	Classification
	Left eye MSE	Right eye MSE		Left eye accuracy
OU-Copula	1.726(0.2307)	1.712(0.2135)	CeCNN	0.779
CeViT	1.275(0.1173)	1.290(0.1083)	CeViT	0.781(0.0158)
CeViT-A	1.261 (0.1083)	1.289 (0.0894)	CeViT-A	0.785 (0.0176)

This article focuses on enhancing OU myopia screening with static UWF fundus images that are observed once. The future interest of practitioners from the Eye & ENT Hospital falls on detecting the evolution of high-myopia and other ocular diseases. This calls for new

longitudinal models to predict future high-myopia status based on dynamic UWF fundus images, which will be our future work.

References

- Avery, R. B. (1977). Error components and seemingly unrelated regressions. *Econometrica: Journal of the Econometric Society*, pages 199–209. [10](#)
- Chen, S., Ge, C., Tong, Z., Wang, J., Song, Y., Wang, J., and Luo, P. (2022). Adapt-former: Adapting vision transformers for scalable visual recognition. *Advances in Neural Information Processing Systems*, 35:16664–16678. [18](#)
- Cinelli, L. P., Marins, M. A., Da Silva, E. A. B., and Netto, S. L. (2021). *Variational methods for machine learning with applications to deep networks*, volume 15. Springer. [13](#)
- Djulonga, J., Yung, J., Tschannen, M., Romijnders, R., Beyer, L., Kolesnikov, A., Puigcerver, J., Minderer, M., D’Amour, A., Moldovan, D., et al. (2021). On robustness and transferability of convolutional neural networks. In *Proceedings of the IEEE/CVF Conference on Computer Vision and Pattern Recognition*, pages 16458–16468. [4](#)
- Dosovitskiy, A., Beyer, L., Kolesnikov, A., Weissenborn, D., Zhai, X., Unterthiner, T., Dehghani, M., Minderer, M., Heigold, G., Gelly, S., et al. (2020). An image is worth 16x16 words: Transformers for image recognition at scale. In *International Conference on Learning Representations*. [3](#), [7](#), [11](#), [12](#)
- Engelmann, J., McTrusty, A. D., MacCormick, I. J., Pead, E., Storkey, A., and Bernabeu, M. O. (2022). Detecting multiple retinal diseases in ultra-widefield fundus imaging and data-driven identification of informative regions with deep learning. *Nature Machine Intelligence*, 4(12):1143–1154. [2](#)
- Fan, J., Gu, Y., and Zhou, W.-X. (2024). How do noise tails impact on deep relu networks? *The Annals of Statistics*, 52(4):1845–1871. [5](#)
- Gour, N. and Khanna, P. (2021). Multi-class multi-label ophthalmological disease detection using transfer learning based convolutional neural network. *Biomedical Signal Processing and Control*, 66:102329. [3](#)
- Haarman, A. E., Enthoven, C. A., Tideman, J. W. L., Tedja, M. S., Verhoeven, V. J., and Klaver, C. C. (2020). The complications of myopia: a review and meta-analysis. *Investigative Ophthalmology & Visual Science*, 61(4):49–49. [2](#)
- Han, K., Wang, Y., Chen, H., Chen, X., Guo, J., Liu, Z., Tang, Y., Xiao, A., Xu, C., Xu, Y., et al. (2022). A survey on vision transformer. *IEEE Transactions on Pattern Analysis and Machine Intelligence*, 45(1):87–110. [3](#)
- He, K., Zhang, X., Ren, S., and Sun, J. (2016). Deep residual learning for image recognition. In *Proceedings of the IEEE Conference on Computer Vision and Pattern Recognition*, pages 770–778. [23](#)
- Hendrycks, D. and Gimpel, K. (2016). Gaussian error linear units (GELUs). *arXiv preprint arXiv:1606.08415*. [12](#)
- Henriquez, M. A., Izquierdo Jr, L., and Belin, M. W. (2015). Intereye asymmetry in eyes with keratoconus and high ametropia: Scheimpflug imaging analysis. *Cornea*, 34:S57–S60. [2](#), [7](#)

- Hu, E. J., Shen, Y., Wallis, P., Allen-Zhu, Z., Li, Y., Wang, S., Wang, L., and Chen, W. (2022). Lora: Low-rank adaptation of large language models. In *International Conference on Learning Representations*. [12](#)
- Huang, J., Jiao, Y., Liao, X., Liu, J., and Yu, Z. (2024). Deep dimension reduction for supervised representation learning. *IEEE Transactions on Information Theory*, *5*, [13](#)
- Iwase, A., Araie, M., Tomidokoro, A., Yamamoto, T., Shimizu, H., Kitazawa, Y., Group, T. S., et al. (2006). Prevalence and causes of low vision and blindness in a japanese adult population: the tajimi study. *Ophthalmology*, *113*(8):1354–1362. [2](#)
- Kolesnikov, A., Beyer, L., Zhai, X., Puigcerver, J., Yung, J., Gelly, S., and Houlsby, N. (2020). Big transfer (bit): General visual representation learning. In *Computer Vision—ECCV 2020: 16th European Conference, Glasgow, UK, August 23–28, 2020, Proceedings, Part V 16*, pages 491–507. Springer. [4](#)
- Li, B. (2018). *Sufficient dimension reduction: Methods and applications with R*. CRC Press. [13](#)
- Li, B., Li, Y., and Eliceiri, K. W. (2021). Dual-stream multiple instance learning network for whole slide image classification with self-supervised contrastive learning. In *Proceedings of the IEEE/CVF Conference on Computer Vision and Pattern Recognition*, pages 14318–14328. [6](#)
- Li, Y., Huang, Q., Zhong, C., Yang, D., Li, M., Welsh, A., Liu, A., Fu, B., Liu, C. C., and Zhou, X. (2024). OUCopula: Bi-Channel Multi-Label Copula-Enhanced Adapter-Based CNN for Myopia Screening Based on OU-UWF Images. *Proceedings of the Thirty-Third International Joint Conference on Artificial Intelligence (IJCAI-24)*, pages 5927–5935. [3](#), [7](#), [14](#), [22](#)
- Liu, Z., Xu, Y., Xu, Y., Qian, Q., Li, H., Ji, X., Chan, A., and Jin, R. (2022). Improved fine-tuning by better leveraging pre-training data. *Advances in Neural Information Processing Systems*, *35*:32568–32581. [5](#)
- Lu, J., Zhou, H., Shi, Y., Choe, J., Shen, M., Wang, L., Chen, K., Zhang, Q., Feuer, W. J., Gregori, G., et al. (2022). Interocular asymmetry of choroidal thickness and vascularity index measurements in normal eyes assessed by swept-source optical coherence tomography. *Quantitative Imaging in Medicine and Surgery*, *12*(1):781. [2](#)
- Midena, E., Marchione, G., Di Giorgio, S., Rotondi, G., Longhin, E., Frizziero, L., Pilotto, E., Parrozzani, R., and Midena, G. (2022). Ultra-wide-field fundus photography compared to ophthalmoscopy in diagnosing and classifying major retinal diseases. *Scientific Reports*, *12*(1):19287. [2](#)
- Oh, R., Lee, E. K., Bae, K., Park, U. C., Yu, H. G., and Yoon, C. K. (2023). Deep learning-based prediction of axial length using ultra-widefield fundus photography. *Korean journal of ophthalmology: KJO*, *37*(2):95. [2](#)
- Paszke, A., Gross, S., Massa, F., Lerer, A., Bradbury, J., Chanan, G., Killeen, T., Lin, Z., Gimelshein, N., Antiga, L., et al. (2019). Pytorch: An imperative style, high-performance deep learning library. *Advances in neural information processing systems*, *32*. [4](#)
- Prucha, I. R. (1984). On the asymptotic efficiency of feasible aitken estimators for seemingly unrelated regression models with error components. *Econometrica: Journal of the Econometric Society*, pages 203–207. [16](#)
- Rebuffi, S.-A., Bilen, H., and Vedaldi, A. (2017). Learning multiple visual domains with residual adapters. *Advances in neural information processing systems*, *30*. [7](#)

- Sankaridurg, P., Holden, B., Chen, X., Ho, A., Li, L., Donovan, L., and Ge, J. (2013). Correlation in myopia progression between right and left eyes in chinese children with myopia. *Investigative Ophthalmology & Visual Science*, 54(15):5712–5712. [2](#), [7](#)
- Shen, G., Jiao, Y., Lin, Y., Horowitz, J. L., and Huang, J. (2024). Nonparametric estimation of non-crossing quantile regression process with deep requ neural networks. *Journal of Machine Learning Research*, 25(88):1–75. [5](#)
- Shi, Z., Wang, T., Huang, Z., Xie, F., and Song, G. (2021). A method for the automatic detection of myopia in optos fundus images based on deep learning. *International Journal for Numerical Methods in Biomedical Engineering*, 37(6):e3460. [2](#)
- Sklar, M. (1959). Fonctions de repartition an dimensions et leurs marges. *Publ. inst. statist. univ. Paris*, 8:229–231. [4](#)
- Song, P. X.-K., Li, M., and Yuan, Y. (2009). Joint regression analysis of correlated data using gaussian copulas. *Biometrics*, 65(1):60–68. [5](#)
- Teng, J., Ma, J., and Yuan, Y. (2022). Towards understanding generalization via decomposing excess risk dynamics. In *International Conference on Learning Representations*. [19](#)
- Vaswani, A., Shazeer, N., Parmar, N., Uszkoreit, J., Jones, L., Gomez, A. N., Kaiser, Ł., and Polosukhin, I. (2017). Attention is all you need. *Advances in Neural Information Processing Systems*, 30. [3](#), [7](#)
- Wang, Q., Ma, Y., Zhao, K., and Tian, Y. (2020). A comprehensive survey of loss functions in machine learning. *Annals of Data Science*, pages 1–26. [2](#), [8](#)
- Wang, X., Zhou, L., and Lin, H. (2024). Deep regression learning with optimal loss function. *Journal of the American Statistical Association*, (just-accepted):1–20. [5](#)
- Xiao, Y., Shao, H., Wang, J., Yan, S., and Liu, B. (2024). Bayesian variational transformer: A generalizable model for rotating machinery fault diagnosis. *Mechanical Systems and Signal Processing*, 207:110936. [4](#)
- Xu, Y. and Fan, Y. (2022). Dual-channel asymmetric convolutional neural network for an efficient retinal blood vessel segmentation in eye fundus images. *Biocybernetics and Biomedical Engineering*, 42(2):695–706. [3](#)
- Yang, D., Li, M., Li, W., Wang, Y., Niu, L., Shen, Y., Zhang, X., Fu, B., and Zhou, X. (2022). Prediction of refractive error based on ultrawide field images with deep learning models in myopia patients. *Frontiers in Medicine*, 9:834281. [2](#)
- Yew, S. M. E., Chen, Y., Goh, J. H. L., Chen, D. Z., Tan, M. C. J., Cheng, C.-Y., Koh, V. T. C., and Tham, Y. C. (2024). Ocular image-based deep learning for predicting refractive error: A systematic review. *Advances in Ophthalmology Practice and Research*, 4(3):164–172. [2](#)
- Zhang, S., Chen, Y., Li, Z., Wang, W., Xuan, M., Zhang, J., Hu, Y., Chen, Y., Xiao, O., Yin, Q., et al. (2024). Axial elongation trajectories in chinese children and adults with high myopia. *JAMA ophthalmology*, 142(2):87–94. [2](#)
- Zhong, C., Li, Y., Yang, D., Li, M., Zhou, X., Fu, B., Liu, C. C., and Welsh, A. (2024). CeCNN: Copula-enhanced convolutional neural networks in joint prediction of refraction error and axial length based on ultra-widefield fundus images. *The Annals of Applied Statistics*, In press. [2](#), [4](#), [8](#), [14](#), [16](#), [22](#)